

# Fabrication of Smooth Surfaces based on Mask Projection Stereolithography

Yayue Pan, Yong Chen\*, Chi Zhou  
Epstein Department of Industrial and Systems Engineering  
University of Southern California, Los Angeles, CA 90089

\*Corresponding author: [yongchen@usc.edu](mailto:yongchen@usc.edu), (213) 740-7829

## Abstract

The surface finish is critical for applications such as micro-fluid mixing and self-assembly that requires smooth fluidic flow and mechanical rotation respectively. However, in layer-based additive manufacturing processes, it is well known that the stair-stepping effect exists in the fabricated surfaces since a three-dimensional model is approximated by a set of two-dimensional layers. The fabricated surfaces are especially poor for the ones that are close to the horizontal plane. In this paper a novel approach for achieving improved surface finish has been presented for the mask-image-projection-based Stereolithography (MIP-SL) process. Theoretical models and parameter characterization are presented with experimental verification. The developed approaches have been incorporated in the process planning of the MIP-SL process. Multiple test cases based on various types of curved surfaces have been performed. A comparison of the built results based on the traditional and the newly developed approaches has been discussed to illustrate the effectiveness of our method.

**Keywords:** Additive manufacturing, surface finish, layer stair-stepping, mask projection stereolithography.

## 1. Introduction

One of the major problems in the layer-based additive manufacturing (AM) processes is the poor surface finish associated with the layer stair-stepping effect. As shown in Figure 1, a given three-dimensional (3D) model is first sliced into a set of two-dimensional (2D) layers. By stacking the 2D layers together, a physical part can be fabricated in an AM process to approximate the original computer-aided design (CAD) model. Due to the use of 2D layers, the fabricated part surfaces especially the ones whose normals are close to the building direction (Z axis) may have big approximation errors. Such poor surface quality limits the use of AM in applications that require smooth surfaces, e.g. the fabrication of 3D micro-channels in microfluidic systems or various assembly features in high-precision products.

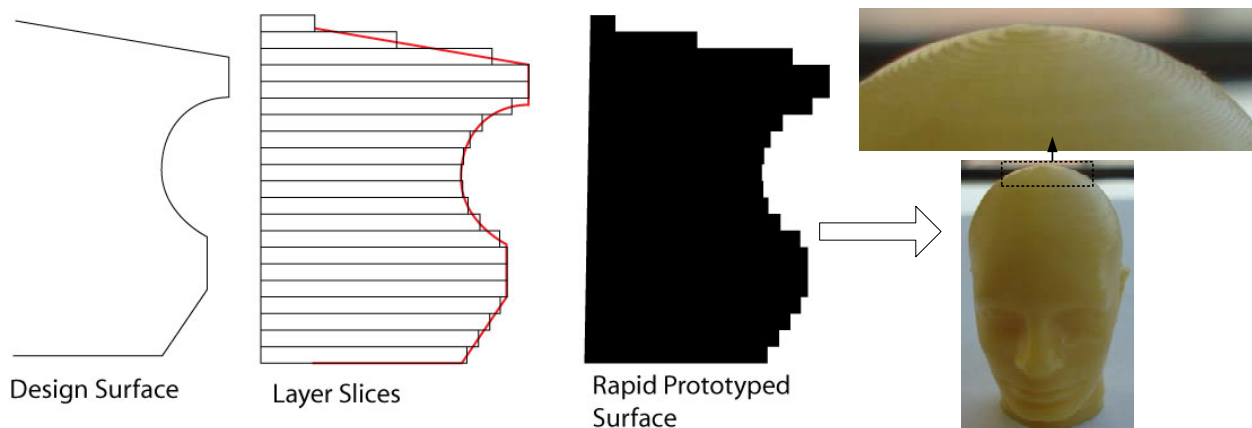


**Figure 1.** An illustration of the layer-based additive manufacturing processes and related stair-stepping effect.

Since the approximation error depends on the layer thickness used in the slicing of a 3D model, a dominant approach for addressing the stair-stepping effect in AM is to reduce the layer thickness. For example, the layer thickness typically used in a Stereolithography Apparatus (SLA) system is 0.1 mm

while the layer thickness used in the latest developed inkjet-based systems (e.g. the ones from Objet Geometries Ltd) can be as small as 0.012mm. While the thinner layers in comparison always have less stair-stepping problems, the use of such ultra-thin layer thickness also significantly slows down the building process. In addition to the big sacrifice in building speed, it is also very difficult for AM processes such as SLA to significantly reduce its layer thickness since the spreading of liquid resin into uniform ultra-thin layers is well-know challenging.

In this paper, we present an alternative approach for achieving smooth surfaces in the SLA-related processes. The AM process considered in this paper is the mask-image-projection-based stereolithography (MIP-SL). An illustration of the MIP-SL process is shown in Figure 1.a. The MIP-SL process is quite similar to the SLA process. However, a Digital Micromirror Device (DMD) instead of a laser is used in the MIP-SL process. A DMD is a microelectromechanical system (MEMS) device that enables one to simultaneously control  $\sim 1$  million small mirrors to turn on or off a *pixel* at over 5 KHz. Hence mask images can be dynamically defined and projected on a surface area. By replacing a laser with a DMD, the MIP-SL process can be much faster than the SLA process.

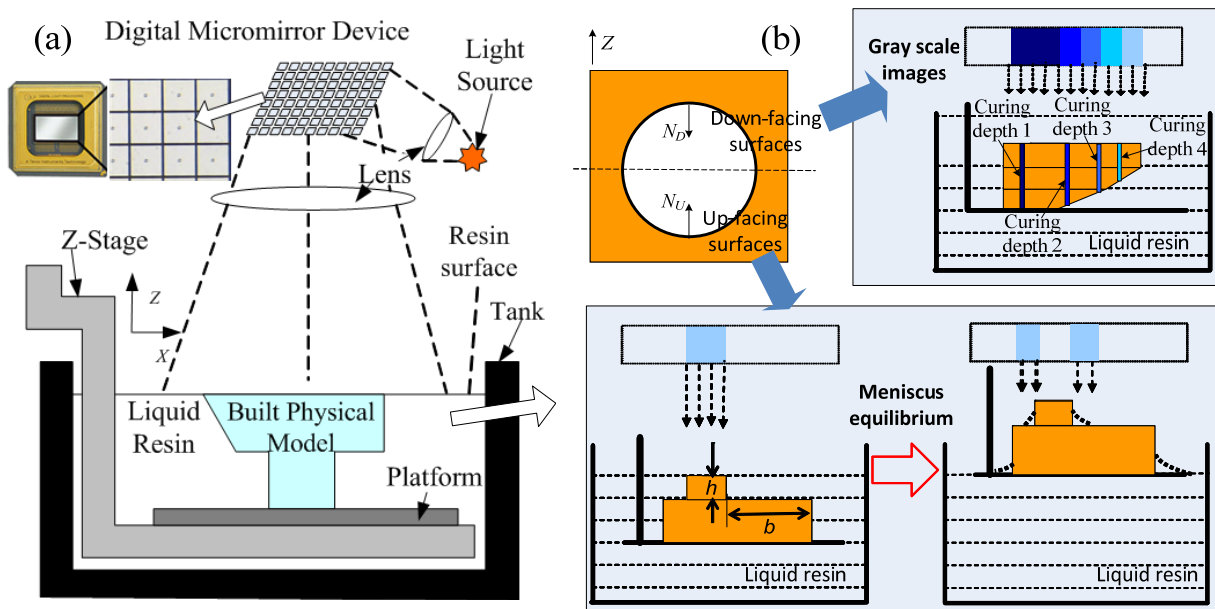


**Figure 2.** An illustration of the MIP-AM process and related approaches for improving its surface finish.

Based on the  $Z$  axis and its surface normal  $N$ , all the surfaces in a 3D model can be classified into: (1) vertical surfaces ( $N \cdot Z = 0$ ), (2) down-facing surfaces ( $N \cdot Z < 0$ ), and (3) up-facing surfaces ( $N \cdot Z > 0$ ). There is no need to specially consider the vertical surfaces since they generally do not contribute to the stair-stepping effect. For the other two types of surfaces, our approaches for improving their surface finishes are shown in Figure 2.b.

- (1) A gray scale image approach has been developed for the fabrication of smooth down-facing surfaces. As shown in Figure 2.b-(top), the key idea of the approach is to use a fine  $Z$  resolution to sample a given down-facing surface. Hence the curing depth at each pixel can be represented by a cure depth that has a higher resolution than the layer thickness. Accordingly a gray scale value at a pixel can be set to provide the desired energy input for the related curing depth. Consequently a gray scale image will be computed for all the down-facing surfaces in the MIP-AM process.
- (2) A meniscus equilibrium approach has been developed for the fabrication of smooth up-facing surfaces. As shown in Figure 2.b-(bottom), the key idea of the approach is to closely match the fluid interfaces at the corners of intersecting planes to the related curved surfaces in the input geometry. Hence, liquid meniscus will be formed at the corners when the cured layers emerge out

from the liquid. The shapes of the menisci depend on the contact horizontal and vertical surfaces, and can be modeled by considering the effects of capillarity, suction by gravity, multilayer adsorption and the boundary conditions [1, 2]. Accordingly a process optimization problem can be formulated in order to match the menisci to the given curved surfaces.

Compared to the use of ultra-thin layers that significantly elongates the building time, the developed techniques enable a much bigger layer thickness to be used while achieving similar surface finish requirement. Hence significantly reduced building time could be expected in the MIP-AM process. To explain both techniques in more details, the remainder of the paper is organized as follows. The building technique developed for up-facing surfaces will be discussed first. Section 2 presents the models of formed meniscus in various cases. Accordingly the process planning for building smooth up-facing surfaces is presented in Section 3. The building technique developed for down-facing surfaces will then be presented. Section 4 presents the curing model for pixels with different gray scale values. Based on it, the process planning for building smooth down-facing surfaces is presented in Section 5. The experimental setup for performing physical experiments is presented in Section 6. The test results for various curved surfaces are discussed in Section 7. Finally, conclusion with future work is drawn in Section 8.

## 2. Modeling Formed Menisci in MIP-SL

The formation of the interfacial profile of the equilibrium meniscus that is attached to intersecting surfaces is first discussed. Such understanding and related mathematic models will provide the theoretical basis for the process planning and smoothness control of the up-facing surfaces. As shown in Figure 3.a, given a pair of walls, suppose the length of the horizontal plane is  $b$ , and the height of the vertical plane is  $h$ . With a finite horizontal plane, the maximum range of the fluid that can rise up on an infinite vertical plane  $y(x=0, xlength=b)$  is  $h_c$ . Similarly, with a finite vertical plane, the maximum range of the fluid that can extend along an infinite horizontal plane  $x(y=0, ylength=h)$  is  $b_0$ .

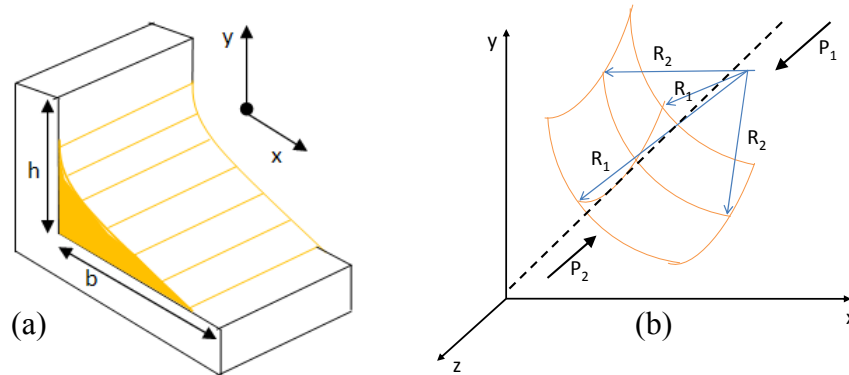


**Figure 3.** Meniscus wetting to intersecting plane surfaces and fluid interface profile.

Previous research on determining equilibrium shapes of fluid interfaces has been performed [3-7]. The *Young-Laplace* (YL) equation is the most widely accepted physical analysis of equilibrium meniscus shape. In the analysis, two types of forces, surface tension and pressure, are taken into account. The surface tension is defined with respect to a specific photopolymer resin. It is a thermodynamic quantity measuring the energy required to expand the area of the gas-liquid interface. As shown in Figure 3.b, the YL equation relates the pressure difference  $\Delta P$  across a fluid interface within a gravitational field to the curvature of the interface and the interfacial tension by:

$$\Delta P = P_1 - P_2 = -\rho gy = \gamma_{12} \times \left( \frac{1}{R_1} + \frac{1}{R_2} \right) ; \quad (2.1)$$

where  $P_1$  and  $P_2$  are the pressures on either side of the interface between resin and air,  $g$  is gravity acceleration,  $y$  is the height of the meniscus above the horizontal plane surface,  $\gamma_{12}$  is the interfacial tension,  $R_1$  and  $R_2$  are the radii of curvature of the fluid interface. If  $R_1$  can be considered as infinite, the problem is simplified to a 2D case. Thus the following equation (2.2) can be derived from Eq. (2.1):

$$\rho g y - \gamma_{12} \times \frac{\ddot{y}}{(1 + \dot{y}^2)^{2/3}} = 0; \quad \dot{y} = \frac{dy}{dx}; \quad \ddot{y} = \frac{d\dot{y}}{dx} \quad (2.2)$$

The interfacial tension  $\gamma$  has a relation with the capillary height  $h_c$  and the contact angle  $\theta$  as shown in Equation (2.3).

$$h_c^2 = 2 \frac{\gamma}{\rho g} (1 - \sin \theta); \quad (2.3)$$

So Equation (2.4) can be developed according to Equation (2.2) and (2.3).

$$\rho g y - \frac{1}{2} h_c^2 \times \frac{\rho g \ddot{y}}{(1 - \sin \theta)(1 + \dot{y}^2)^{2/3}} = 0 \quad (2.4)$$

## 2.1 Process Parameter Calibration

The contact angle  $\theta$  in Eq. (2.4) is the angle at which the liquid resin interface meets the solidified resin surface. Specific to the given liquid and solid system, the contact angle is determined by the interactions across the three interfaces, including liquid resin, solidified resin and air. Researchers reported that  $\theta$  is observed to be independent of volume and gravity and depends only on the surface tension [8, 9]. The capillary height  $h_c$  is the maximum height that the fluid can reach on an infinite vertical wall.  $h_c$  is a characteristic length for the fluid subject to gravity and surface tension.

Both parameters ( $\theta$  and  $h_c$ ) can be experimentally measured. Based on different  $b$  and  $h$  values, a set of experiments have been designed. Test parts with designed intersecting horizontal and vertical surfaces were built using the MIP-SL process. After curing the horizontal and vertical surfaces, the part is lifted up from the liquid resin slowly. Liquid meniscus in contact with the intersecting surfaces will be formed. After a long waiting time, the liquid volume will reach equilibrium over the horizontal wettable surface area. A mask image is then projected on the meniscus area to cure the liquid resin. The shape of the formed menisci can thus be captured in the built part. A set of parts with different sizes of horizontal and vertical planes have been built. Two of such built parts are shown in Figure 4. Based on the experiments, the contact angle  $\theta$  and the capillary height  $h_c$  can be measured. For the liquid resin used in our experiments (envisionTEC SI500, Ferndale, MI), we estimated that  $\theta=25^\circ$ , and  $h_c=1.40\text{mm}$ .

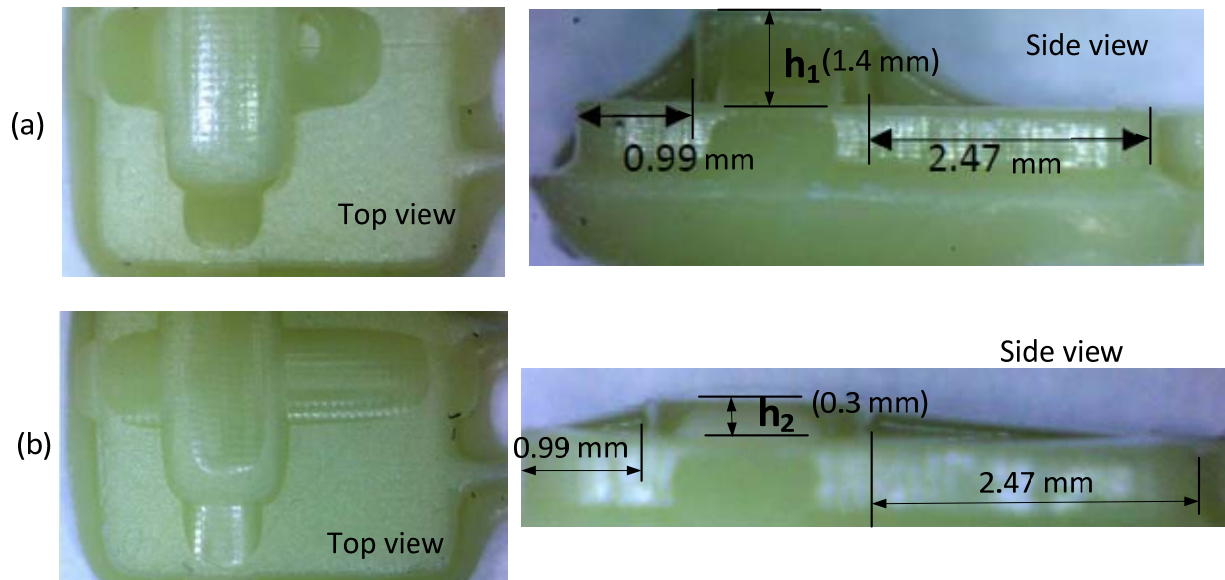


**Figure 4.** Two built parts with different  $b$  and  $h$  values for measuring surface tension parameters.

## 2.2 Meniscus Shape Analysis and Simulation

In the MIP-SL process, let  $h$  denote the height of the vertical plane and  $b$  be the length of the horizontal plane.  $h_c$  and  $b_0$  denote the maximum range the liquid can reach on the vertical and horizontal plane respectively. The formed meniscus shapes for different  $b$  and  $h$  values can be analyzed based on the following scenarios:

- (1) Case 1:  $h > h_c; b > b_0$ ;
- (2) Case 2:  $h < h_c; b > b_0$ ;
- (3) Case 3:  $h > h_c; b < b_0$ ; and
- (4) Case 4:  $h < h_c; b < b_0$ .

Different boundary conditions can be derived for each scenario, which are discussed as follows.

**(1) Case 1:** both  $h$  and  $b$  can be considered as infinite. The related boundary conditions are:

$$\dot{y}(x=0) = -c \tan \theta = -c \tan 25^\circ = -2.14129; \quad x(0) = b = \infty \quad (2.5)$$

Using the governing equation (2.4) and boundary conditions (2.5), the height of the fluid can reach on the vertical wall is calculated to be 1.398372mm, which agrees well with the experiment result of 1.40 mm. We used Matlab (MathWorks, Natick, MA) to solve this problem and plotted the result as shown in Figure 5.a.

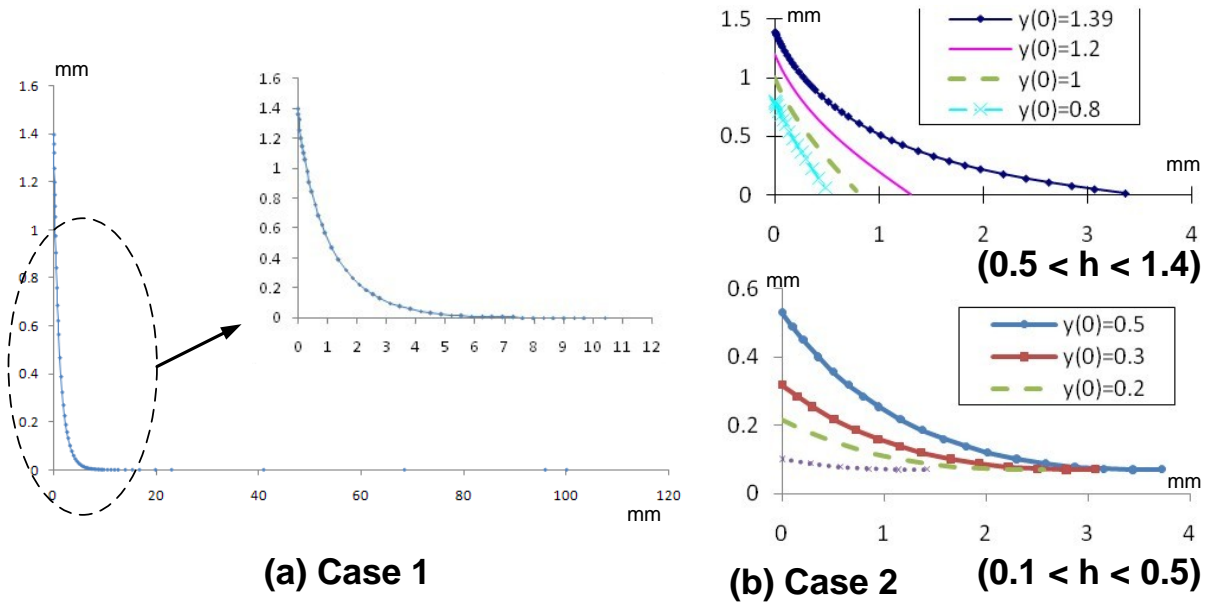


**Figure 5.** Plotting results of the meniscus profile in cases 1 and 2.

**(2) Case 2:**  $h$  is smaller than  $h_c(x=\infty)$ , and  $b$  can be considered as infinite. Hence the curvature of the meniscus is decided by  $h$ . The boundary conditions are as follows.

$$\begin{aligned} \dot{y}(x=0) &= -c \tan \theta = -c \tan 25^\circ = -2.14129; \quad y(0) = h; \\ \dot{y}(y=0) &= -c \tan \theta \leq -c \tan 65^\circ = -0.466038; \end{aligned} \quad (2.6)$$

In this case, the length of the fluid extended on the horizontal plane  $b_0$  is dependent on the value of  $h$ , namely,  $b_0 = f(h)$ . The meniscus shapes with different  $h$  were estimated by solving the governing equation (2.4) and the boundary conditions described in equation (2.6) using Matlab. The plotting results of different  $h$  values are shown in Figure 5.b.

**(3) Case 3:**  $h$  is bigger than  $h_c(x=\infty)$  and  $b$  is smaller than  $b_0$ . Thus the curvature of the meniscus is decided by  $b$ . The boundary conditions are as follows.

$$\begin{aligned} \dot{y}(x=0) &= -c \tan \theta = -c \tan 25^\circ = -2.14129; \\ \dot{y}(y=0) &= -c \tan \theta \leq -c \tan 65^\circ = -0.466038; \\ y(b) &= 0 \end{aligned} \tag{2.7}$$

Based on the governing equation (2.4) and the boundary conditions Equation (2.7), the meniscus shapes can be computed in Matlab. Figure 6 shows the plotting results for different  $b$  values.

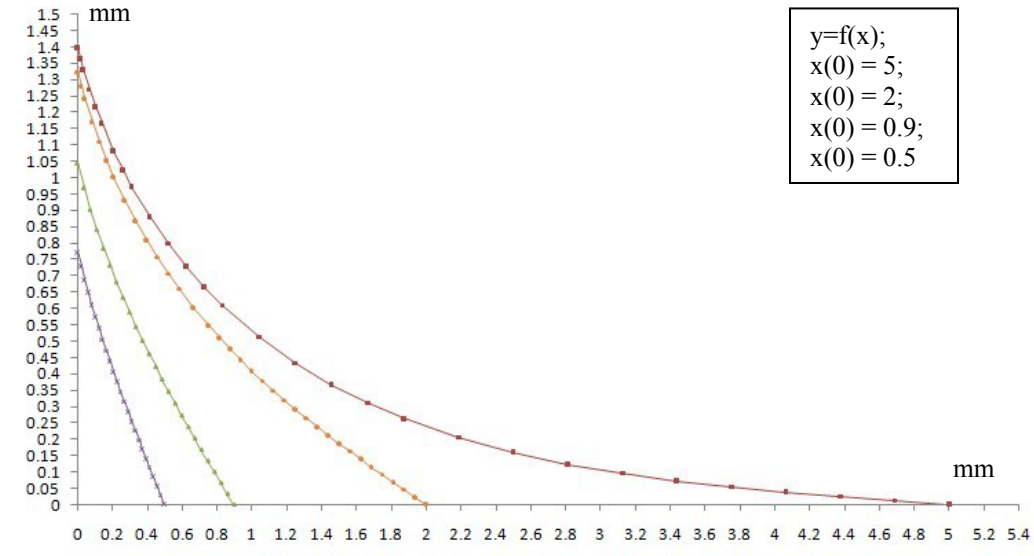


Figure 6. Plotting result of meniscus profile in Case 3.

(4) **Case 4:**  $h$  is smaller than  $h_c(x=\infty)$ , and the length of the horizontal plane  $b$  is smaller than  $b_0$ . Hence the curvature of the meniscus is decided by both  $b$  and  $h$ . The problem follows the boundary conditions:

$$y(0) = h, y(b) = 0 \tag{2.8}$$

The meniscus shape can be calculated for different  $b$  and  $h$  values. Three examples by using Matlab to solve the mathematic model and the related boundary conditions are shown in Figure 7.

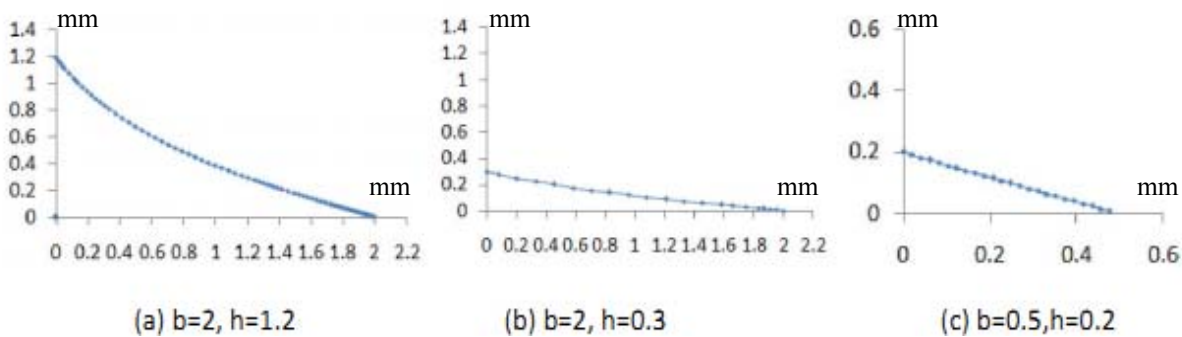
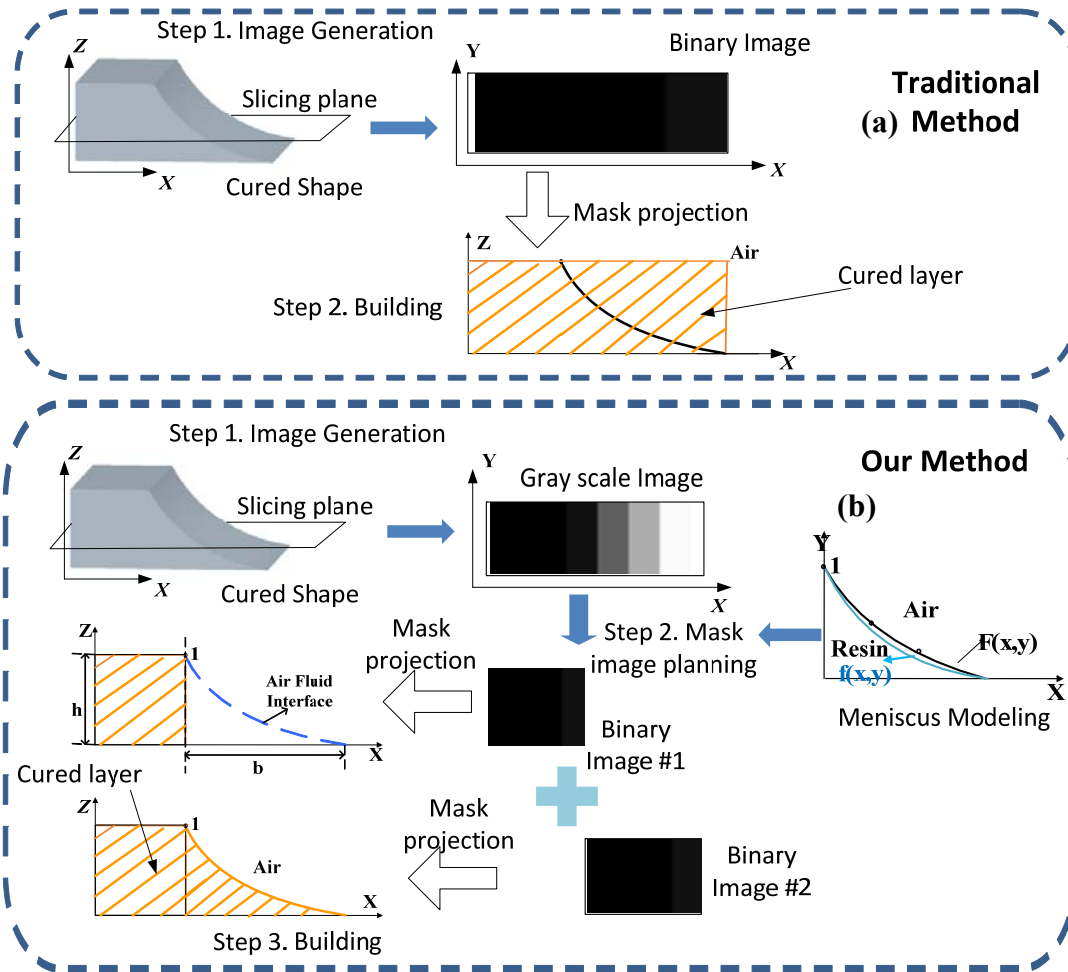


Figure 7. Plotting result meniscus profile in Case 4.

### 3. Process Planning for Building Smooth Up-facing Surfaces

Suppose an input 3D CAD model with curved up-facing surfaces is given as shown in Figure 8.a. The traditional additive manufacturing method will slice the model into multiple 2D layers based on a given layer thickness. One mask image will be generated for each layer in the MIP-SL process to cure the related 2D shape. Consequently the built part will inevitably have stair-stepping defects.



**Figure 8.** Comparison between the traditional and the meniscus equilibrium methods.

In comparison, Figure 8.b illustrates the major steps of the meniscus equilibrium method for achieving smoother up-facing surfaces. For a specific layer  $i$ ,  $c(x, y)$  is computed which represents the ratio of the Z-height at the location  $(x, y)$  to the layer thickness  $L_T$ . Similar to [10], a sliced image with gray scale values can be generated for each layer. Accordingly the thickness at pixel  $(x, y)$  is  $c(x, y) \times L_T$ . Hence instead of a binary layer image, the sliced image has pixels with ratios  $c(x, y)$  which are continuous and  $c(x, y) \in [0, 1]$ . The original gray scale image can be split into two mask images such that the mask image<sub>1</sub> can cure a portion of layer  $i$  that will be used in forming meniscus while the mask image<sub>2</sub> can be used in curing the formed meniscus. Note it is not necessary to use the meniscus equilibrium approach for each layer. Depending on the given geometry, menisci can be formed and cured after multiple layers.

As discussed in the meniscus mathematical model, two important parameters in determining the shape of the meniscus profile are  $h$  and  $b$ . Thus the planning of image<sub>1</sub> and image<sub>2</sub> can change the setting of  $h$  and  $b$ , which lead to different approximation errors between the meniscus profiles and the desired shapes. An illustration example is given in Figure 9.a. For given shape boundary as shown in black lines, two sets of mask images (image<sub>1</sub> and image<sub>2</sub>) can be used, which define two vertical walls as shown in brown lines. Accordingly the formed menisci will have different profiles due to different  $b$  or  $h$  values as shown in Figure 9.a.

In order to generate desired MIP-SL process plan to ensure the meniscus shapes match the given curved geometry, the process planning for the up-facing surfaces can be mathematically defined. Two types of errors need to be considered including the shape and curvature approximation errors. The shape approximation errors  $\epsilon_a$  can be computed by comparing the difference between the meniscus profile  $f(x)$

and the desired geometry profile  $F(x)$ . The curvature approximation error  $\varepsilon_c$  can be computed by comparing the first derivative values of  $f(x)$  and  $F(x)$ . Typically the profile is continuous within each meniscus while there may exist discontinuity among neighboring menisci. Hence the goal in the process planning is to prepare a set of mask images such that the approximation errors can be within a given acceptable region  $[0, \varepsilon_{a0}]$  and  $[0, \varepsilon_{c0}]$ .

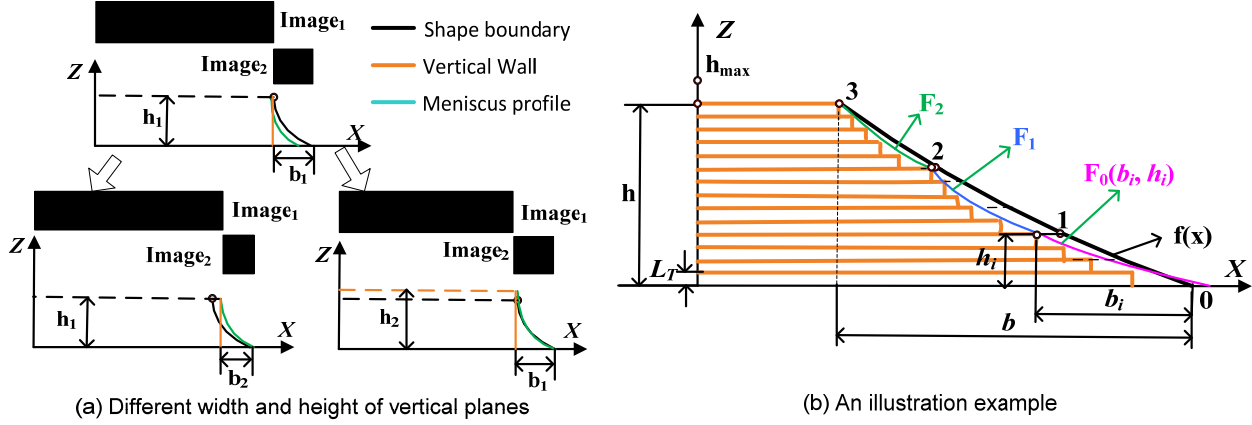


**Figure 9.** An illustration of the process planning problem for the meniscus equilibrium method.

The related problem can be formulated as follows:

**Input:** A curve surface  $f(x, h)$  and a layer thickness.

**Find:** A set of  $b_i$  and  $h_i$

**Satisfy:**

$$F_i(x) = F(b_i, h_i)$$

$$\varepsilon_a = \int_{x_1}^{x_2} |f(x) - F_i(x)| dx \approx \sum_{i=0}^n \nabla d_i;$$

$$\varepsilon_c = \sum_{i=0}^n |\dot{F}_{i+1} - \dot{F}_i|;$$

$$\max(\varepsilon_a) < \varepsilon_{a0} \text{ and } \max(\varepsilon_c) \leq \varepsilon_{c0}, \text{ or } \sum \varepsilon_a < \varepsilon_{a0} \text{ and } \sum \varepsilon_c < \varepsilon_{c0};$$

$$x_2 - x_1 = \sum b_i; F(x_1) - F(x_2) = \sum h_i. \quad (3.1)$$

As shown in Figure 9.b, suppose a boundary curve  $y = f(x)$  ( $y \in (0, h), x \in (x_1, x_2)$ ) is given. The input curve can be divided into several pieces such that  $h$  in the process planning is smaller than the maximum vertical height  $h_c$  as discussed in the meniscus model. Suppose  $L_T$  is the layer thickness and a sampling distance  $e$  is used in computing the errors of the meniscus profile. An algorithm based on the greedy heuristic can be developed as follows. The meniscus shape in the area of  $y \in (0, h)$  is first estimated and compared with the input geometry. If the errors are within the acceptable ranges,  $P_h$  (i.e. point 3) can be selected as the meniscus point; otherwise, the meniscus shape in the area of  $y \in (0, h - i \times L_T)$ ,  $i = 1, 2, \dots$  are estimated until a meniscus point  $P_{h0}$  is found that satisfies the given approximation error ranges (e.g. point 1). The remaining curve can then be processed in a similar way to identify all the meniscus points  $P_{hi}$  (e.g. points 1, 2, 3). Based on the identified meniscus points, a set of projection images (image<sub>1</sub> and image<sub>2</sub>) can be computed for the building process. Accordingly image<sub>1</sub> can be used in solidifying resin layer by layer. When the current layer number comes to  $h_i$ , the fabricated model will be emerged from the liquid resin; after certain waiting time, related image<sub>2</sub> will then be projected to cure the formed meniscus portion.

#### 4. Modeling Curing Depths Related to Gray Scale Pixels in MIP-AM

The meniscus equilibrium method can only address the up-facing surfaces. To improve the surface finish of down-facing surfaces, a gray scale mask image method has been developed, which is motivated by the idea of the optimized mask image projection [11]. As extensively studies in the SLA process [12], the critical threshold ( $E_c$ ) is a primary parameter for a given photosensitive resin. The liquid resin will be solidified when the exposed energy is bigger than  $E_c$ ; otherwise, the resin will remain as liquid or gel. In addition, the curing depth ( $C_d$ ) is directly related to the energy input  $E$  if  $E > E_c$ . The dependence of  $C_d$  as a function of the exposure  $E$  is generally log-linear [12]. Their relation follows the equation:

$$C_d = D_p \ln\left(\frac{E}{E_c}\right) \quad (4.1)$$

One way to control  $E$  is to adjust the exposure time for a binary projection image [13]. Another approach is to adjust pixels' gray scale values while fixing the exposure time of the projection image. In comparison, the gray scale image approach is easier to control. Hence, in the MIP-AM process, full light intensity will be projected for a pixel of a mask image if its gray scale value  $g = 255$ ; when  $0 < g < 255$ , only partial light intensity will be projected for curing the resin area related to the pixel. Corresponding to a given  $E_c$  and an exposure time  $T$ , a threshold gray scale value  $g_c$  can be identified. An illustration of the gray scale image method is shown in Figure 10. Suppose  $g_c = 75$ . Hence the exposures at pixels  $B$ ,  $C$  and  $D$  whose gray scale values are set as 102, 153 and 204 respectively will lead to cured shapes with different cure depth. No resin will be cured at pixel  $A$  due to its insufficient energy input. In addition, the cure depth of a pixel is required to be bigger than a layer thickness such that sufficient over-cure exists. Hence the current layer can be bonded to the previous layers.

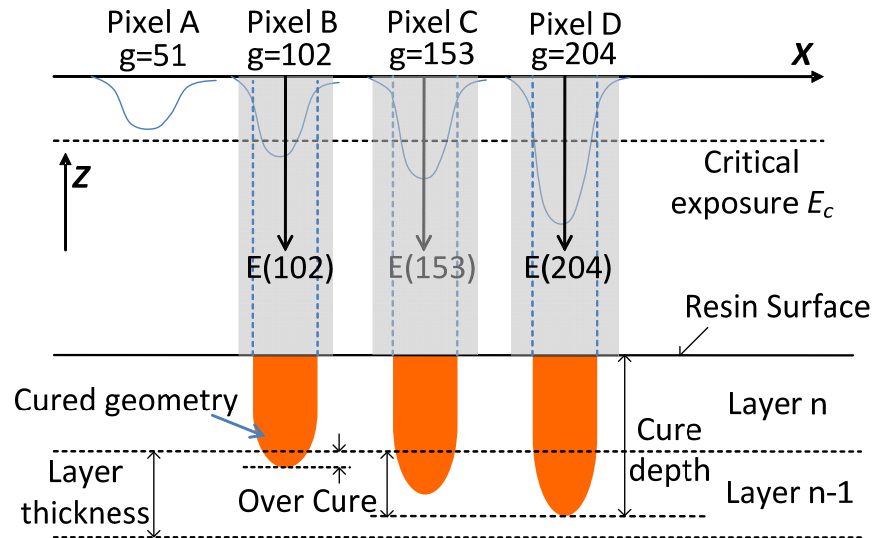


**Figure 10.** Principle of the gray scale image method - the cure depth varies with different gray scale values.

For the liquid resin and the light source used in our testbed, designed experiments have been performed to calibrate the relations between the cure depth and the gray scale values. The CAD model of a designed part is shown in Figure 11.a. In the test, the exposure time was set at 3 seconds. Mask images with different gray scale values were used in curing the top layer. The part was then taken out and the related cured layer thickness  $C_d$  was measured. The recorded  $C_d$  values for different gray scale values are shown in Figure 11.a. The cure depth increases with the set gray scale value. In addition, the gray scale value threshold  $g_c$  is around 76 when  $T = 3$  seconds. For a pixel with  $g < g_c$ , liquid resin was not cured or the cure depth was too small for a given layer thickness (i.e.  $< 0.1$ mm). The relation between  $C_d$  and  $\ln(g)$  has also been computed as shown in Figure 8(c). The relation matches Equation 4.1 quite well and can be approximated by the following equation:

$$F(x) = \begin{cases} 0.521 * \ln(g) - 2.252, & g \geq g_c; \\ 0, & g < g_c \end{cases} \quad (4.2)$$

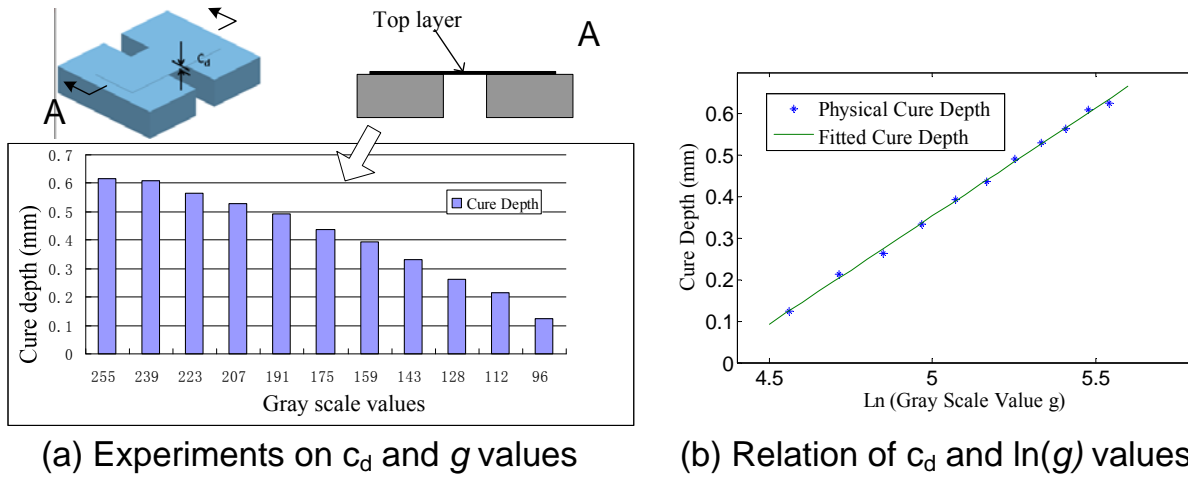


**Figure 11.** Relation between the cure depth with the gray scale value for SI 500 resin with the exposure time of 3s.

Hence by slightly changing the gray scale values of neighboring pixels in a projected mask image, the cure depth related to the pixels can be gradually changed. Thus a higher Z resolution of down-facing surfaces can be achieved, which will lead to improved surface finish. In the process planning for a given 3D model with down-facing surfaces, the cure depth at each pixel needs to be accurately controlled by adjusting its gray scale value. In addition, an upward Z offsetting distance needs to be considered since the range of achievable cure depths (i.e.  $0.1\text{mm} < d < 0.65\text{mm}$ ) is bigger than a layer thickness to ensure the over-cure between layers. Such Z offsetting of down-facing surfaces has also been used in the SLA process [12].

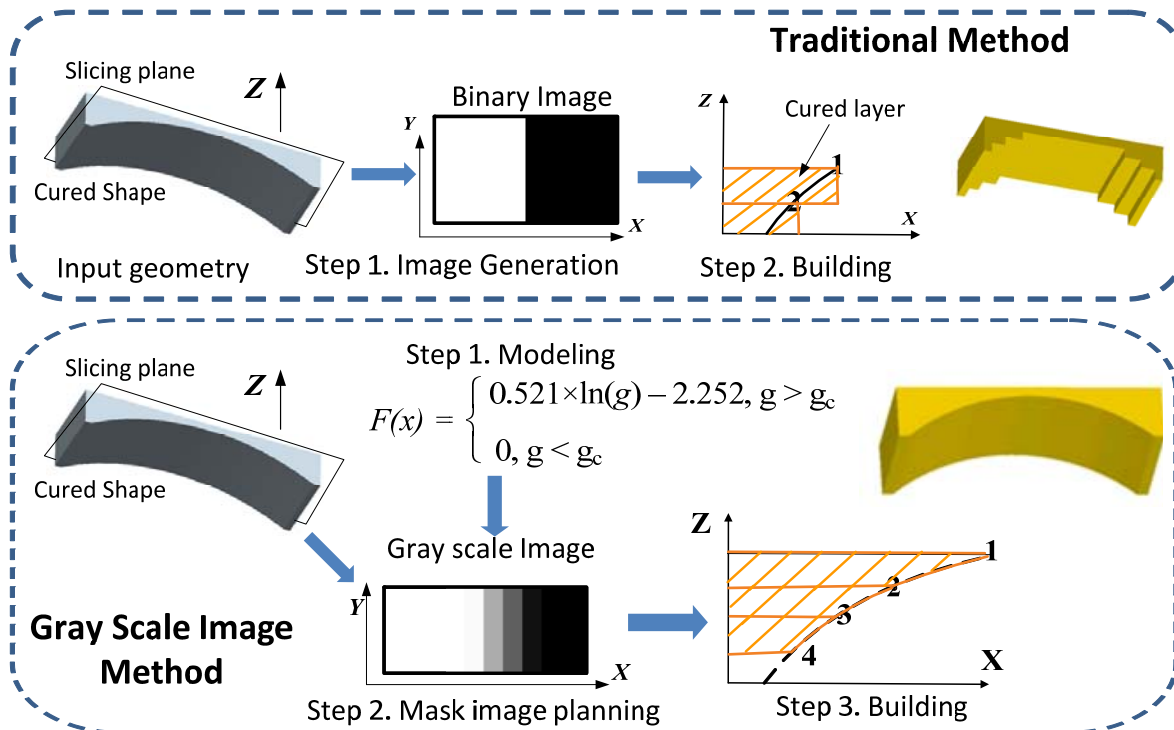


**Figure 12.** Comparison between the traditional and the gray scale image method.

## 5. Process Planning and Smoothness Control for Down-facing Surfaces

The schematic illustration of the traditional and the gray scale image methods are shown in Figure 12. Several layers are reserved as compensation for over-cure. In the traditional method, a set of layers are sliced based on the Z offsetting result. Accordingly binary mask images are used in the MIP-AM process. In the gray scale image method, a compensation Z thickness is calculated based on the minimum and maximum curing depth for gray scale pixels (i.e. 0.1mm and 0.65mm respectively in our test). Hence the desired thickness in each layer is bigger than the minimum achievable curing depth and smaller than the maximum achievable curing depth. Based on the Z offsetting result and the established relation between curing depth and the gray scale values, a mask image with desired gray scale values at all the pixels can be computed. The mask image can then be used in the MIP-AM process for building smooth down-facing surfaces. Figure 13.a shows the related algorithm for generating gray scale mask images. An example is shown in Figure 13.b to illustrate the two main steps, Z offsetting and gray scale image setting.

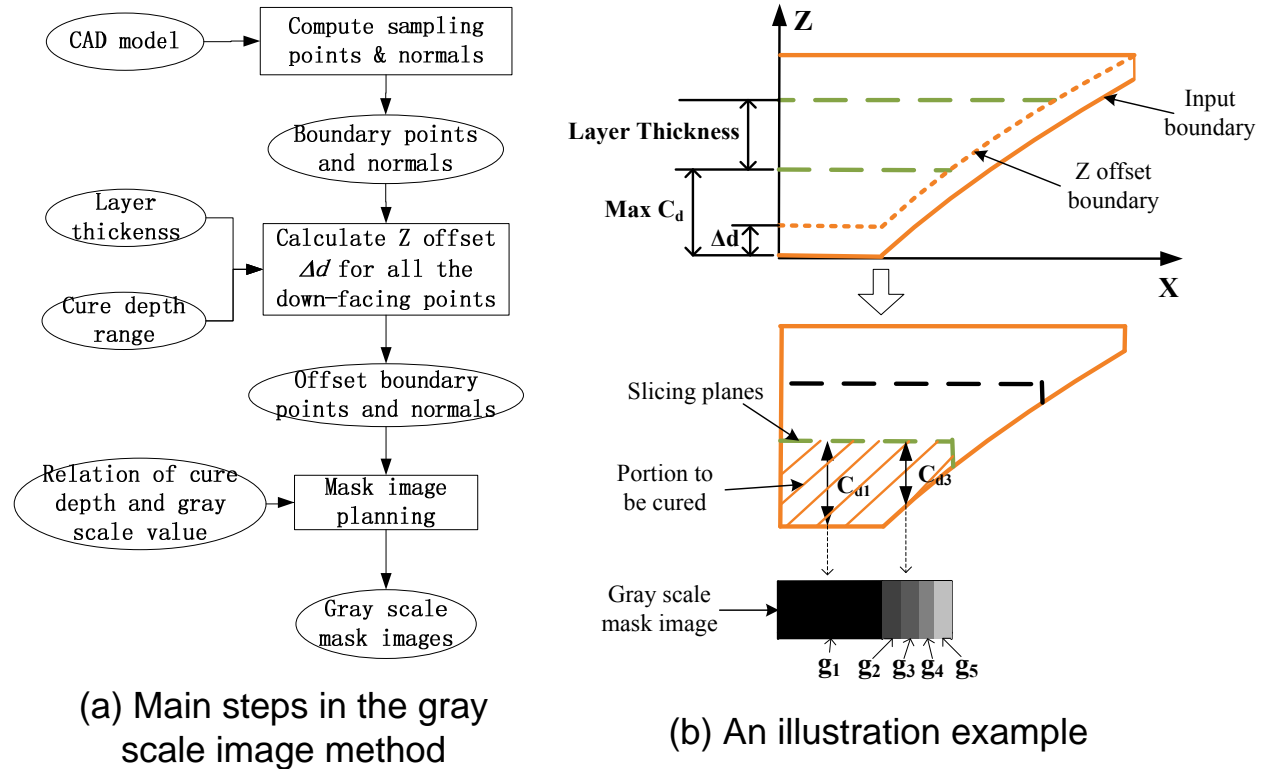


Figure 13. A gray scale image generation algorithm with an illustration example.

## 6. Experimental Setup

A prototype system has been built for verifying the presented approaches. The hardware setup of the developed MIP-SL system is shown in Figure 14.a. In the designed system, an off-the-shelf projector (*Acer H5360*) was used as the projection device. The use of a commercial projector can significantly reduce the prototype cost and simplify the system design. The optical lenses of the projector were modified to reduce the projection distance. Various projection settings including focus, key stone rectification, brightness and contrast were adjusted to achieve a sharp projection image on the designed projection plane. The DMD resolution in our system is  $1024 \times 768$  and the envelope size is set at  $110 \times 82$  mm. Two linear motion stages from Thomson Industries Inc (Radford, VA) are used in the system. One is used as the Z elevator for lifting the build platform; another is used as the sweeper for moving a blade to flatten the resin surface. A high performance 8-axis motion control board KFLOP+SnapAmp 1000 (Dynomotion Inc., Calabasas, CA) was used for driving the linear stages.

Commercially available photocurable resin (envisonTEC *SI500*, Ferndale, MI) was used in the experiments. The exposure time was set at 3 second based on the curing depth analysis. A mask imaging planning and control software system has been developed by using the C++ programming language with Microsoft Visual C++ compiler. The graphical user interface (GUI) of the developed software system is shown in Figure 14.b. The system can load in a STL model, perform process planning and synchronize the mask image projection with desired linear stage motions.

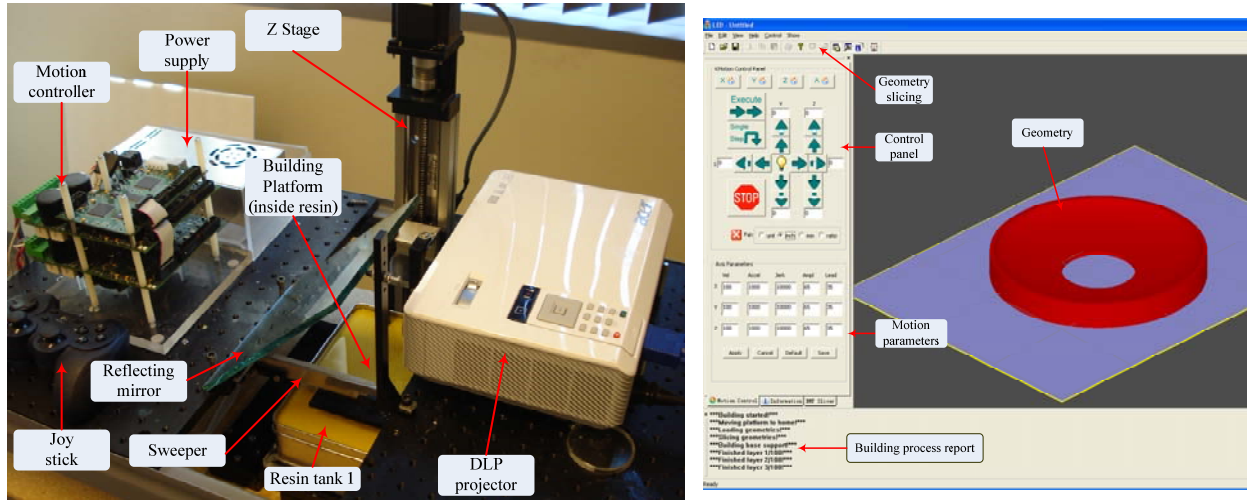


Figure 14. Hardware and software setup of the developed MIP-SL testbed.

## 7. Results and Discussions

A set of test cases have been designed to test the meniscus equilibrium method for up-facing surfaces and the gray scale method for down-facing surfaces. The experimental results are presented as follows.

### 7.1 Tests on Straight Up-facing Surfaces

As shown in Figure 15.a, a CAD model with a slanted surface  $M$  was used in this test. To compare the differences between the traditional and newly developed methods, the surface  $M$  was split into two halves,  $M_1$  and  $M_2$ . The traditional method was used in building the upper half  $M_1$ , and the meniscus equilibrium method was used in building the bottom half  $M_2$ . The same layer thickness (0.1mm) was used in the test. Accordingly a set of mask images were generated by slicing the given CAD model. However, one meniscus point every ten layers was added in set  $\{M\}$  during building  $M_2$ . That is, after every 10 layers have been built, the built part will be raised up by a certain distance (e.g. 1.5mm). After waiting for several minutes, liquid will reach equilibrium. A mask image<sub>2</sub> related to the portion of  $M_2$  within the built 10 layers is then projected to cure the formed meniscuses. The building result is shown in Figure 15.a. It is obvious that the appearance of  $M_2$  portion is much smoother than that of the  $M_1$  portion.

Quantitative measurements have been performed to better understand the surface quality difference. The  $Z$  height of a set of uniformly sampled points on  $M$  was measured by using a digital height gauge with a 0.1mm probe tip. To automate the measuring process, two motion controlled linear stages (Velmex Inc, Bloomfield, NY) were used. In the measurement setup, the built part was fixed on a linear stage to be translated in the  $X$  axis. The digital height gauge was fixed on another linear stage to be translated in the  $Z$  direction. Every time when the probe touches a sampling point on the surface, a height value can be recorded from the digital gauge. To avoid the friction between the probe tip and the slanted surface, the gauge is move away from  $M$  in  $Z$  direction first before the part is fed by a small distance in  $X$  direction. The recorded  $Z$  height values of the sampling points on surface  $M$  is plotted in Figure 15.b. The  $X$  axis denotes a set of uniform-spaced sampling points, where 0 denotes the starting point of the measurement and 400 denotes the 400<sup>th</sup> measuring point. The  $Z$  axis is the readouts from the digital height gauge. The recorded data of the upper half  $M_1$  and the bottom half  $M_2$  are plotted by using blue and red

points respectively. The quantitative comparison shows that the stair-stepping effect of  $M_1$  is much bigger than that of  $M_2$ . We also marked three portions,  $a_1$ ,  $a_2$  and  $a_3$ , on the surface as shown in Figure 15.b. They represent  $M_1$ , the transition between  $M_1$  and  $M_2$ , and  $M_2$  respectively. A precision measurement machine (Sol system from Micro Vu Inc., Windsor, CA) was used in taking microscopic images of these three portions. The captured images are shown in Figure 15.c. The results illustrate that the traditional method will lead to a ragged surface, while the meniscus equilibrium method can effectively eliminate the stair-stepping effect in the MIP-SL process.

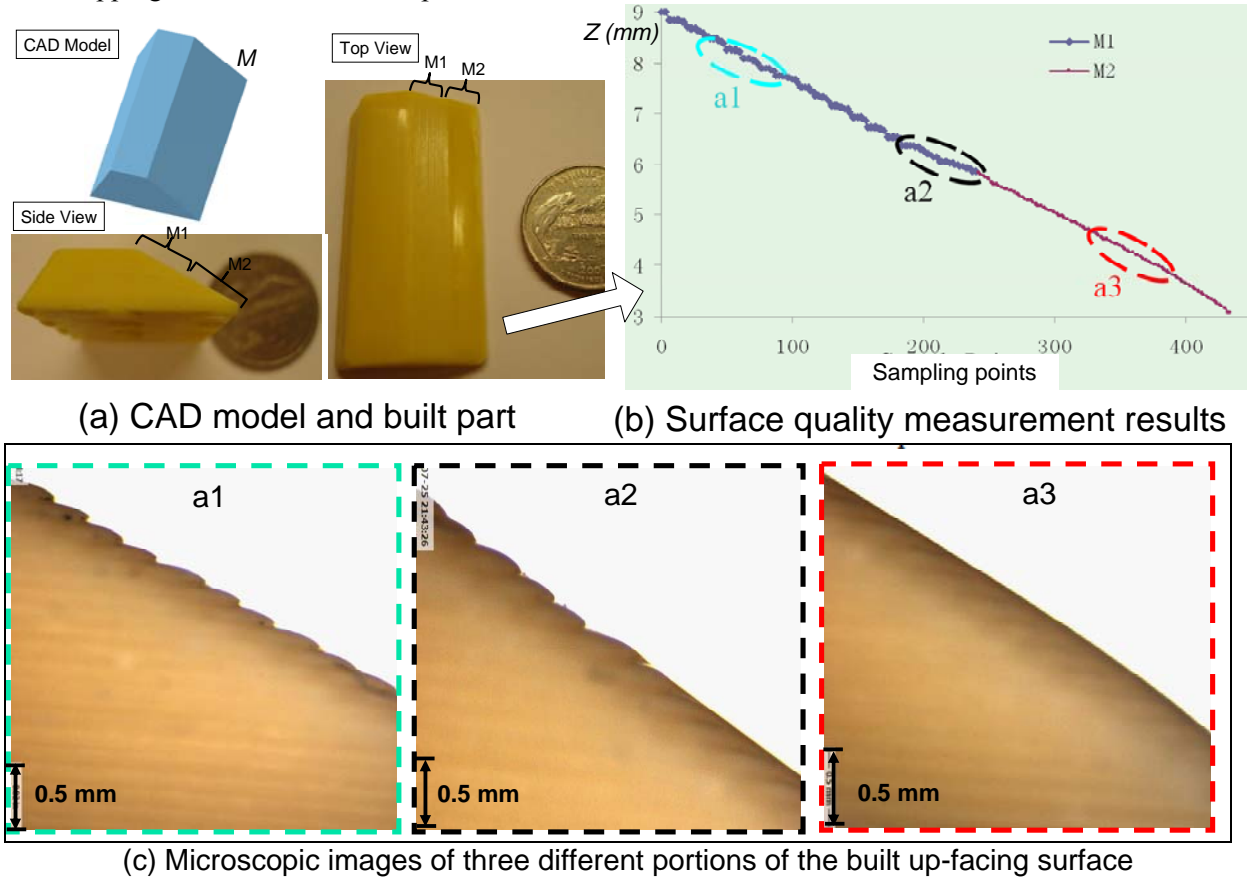
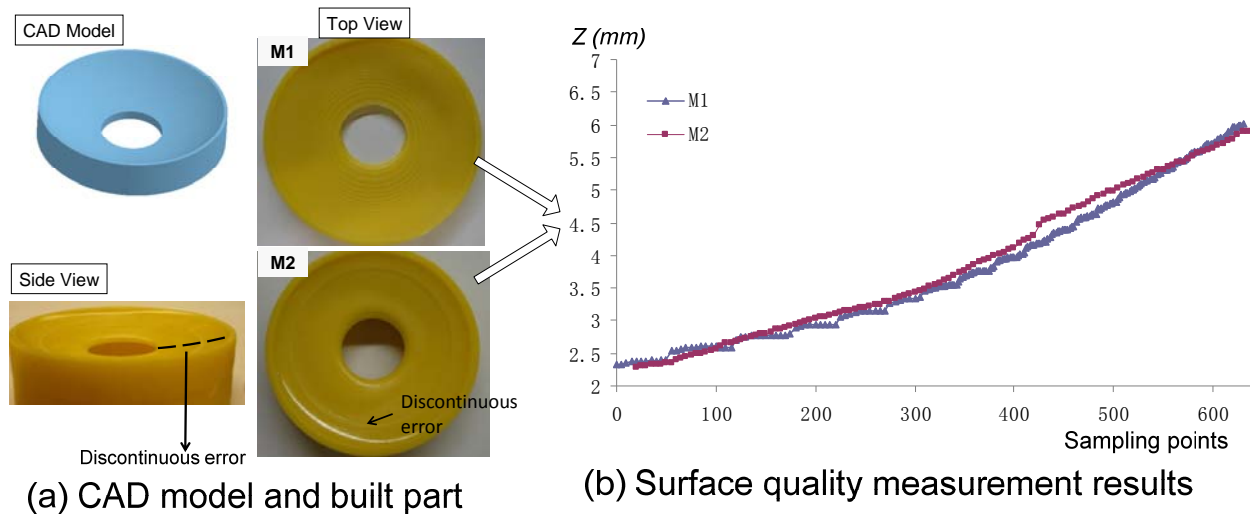


**Figure 15.** A comparison of the built straight up-facing surface based on different methods.

## 7.2 Tests on Curved Up-facing Surfaces – Concave Cases

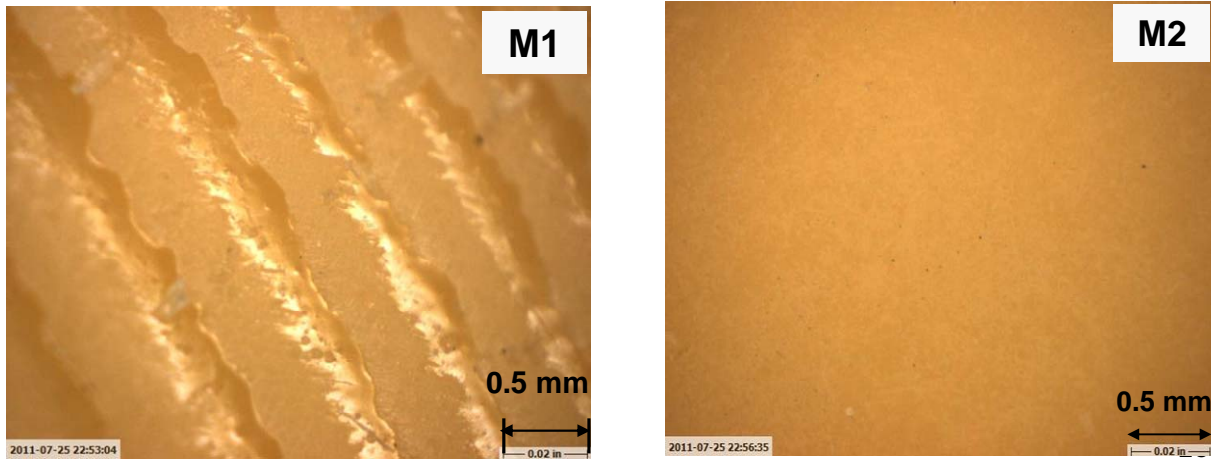
As shown in Figure 16.a, a CAD model with a curved surface  $M$  was used in this test. The same process parameters were used in the traditional and newly developed methods for building the CAD model. The related built results  $M_1$  and  $M_2$  are shown in Figure 16.a. The same measurement procedure as described in Section 7.1 was followed for a quantitative comparison of their surface finishes. The  $Z$  height values of the curved up-facing surface are shown in Figure 16.b. The microscopic images of a portion of  $M_1$  and  $M_2$  are shown in Figure 16.c.

The meniscuses in this test case wet to a cylinder and an intersecting planar surface. The test results verify the capability of the meniscus equilibrium method in fabricating smooth concave up-facing surfaces. One limitation of the developed method is that the given geometry should have an outlet for the liquid resin to flow away such that meniscuses can be formed. In the process planning of the meniscus equilibrium method, there may also be discontinuous error between neighboring meniscuses as shown in Figure 16.a. In order to reduce such error, the generated masks  $image_1$  and the layers at which  $image_2$  will be projected can be adjusted. However, reducing the discontinuous errors may increase the shape approximation error. Hence a balance between the two types of errors needs to be considered. Computing process plans to reduce both errors will be further studied in our future work.



(a) CAD model and built part

(b) Surface quality measurement results



(c) Microscopic images of the built up-facing surfaces

Figure 16. A comparison of the built concave up-facing surfaces based on different methods.

### 7.3 Tests on Curved Up-facing Surfaces – Convex Cases

As shown in Figure 17.a, a CAD model with a curved surface  $M$  was used in this test. The same process parameters were used in building the model by using the traditional and newly developed methods. The related build results  $M_1$  and  $M_2$  are shown in Figure 17.a. The same measurement procedure as described in Section 7.1 was followed for a quantitative comparison of their surface finishes. The  $Z$  height values of the curved up-facing surface are shown in Figure 17.b. The microscopic images of a portion of  $M_1$  and  $M_2$  are shown in Figure 17.c. The test results verify the capability of the meniscus equilibrium method in fabricating smooth convex up-facing surfaces.

### 7.4 Tests on Down-facing Surfaces

As shown in Figure 18.a, a CAD model with a down-facing surface was used in this test. The same process parameters were used in building the model by using the traditional and newly developed methods. To generate gray scale images for building the part, the CAD model was offset by 0.3mm. Accordingly the gray scale value at each pixel was calculated based on the corresponding curing depth. Consequently the computed gray scale images can cure a layer of liquid resin with uneven thicknesses. The related build results  $M_1$  and  $M_2$  are shown in Figure 18.a. The same measurement procedure as described in Section 7.1 was followed for a quantitative comparison of their surface finishes. The  $Z$  height values of the down-facing surface are shown in Figure 18.b. The microscopic images of a portion

of  $M_1$  and  $M_2$  are shown in Figure 18.c. It is obvious from the images that the traditional method can only cure layers with an increment of the given layer thickness. In comparison, the gray scale image method can achieve varying Z heights within one layer. Therefore, the gray scale image method can significantly improve the surface smoothness of down-facing surfaces in the MIP-SL process.

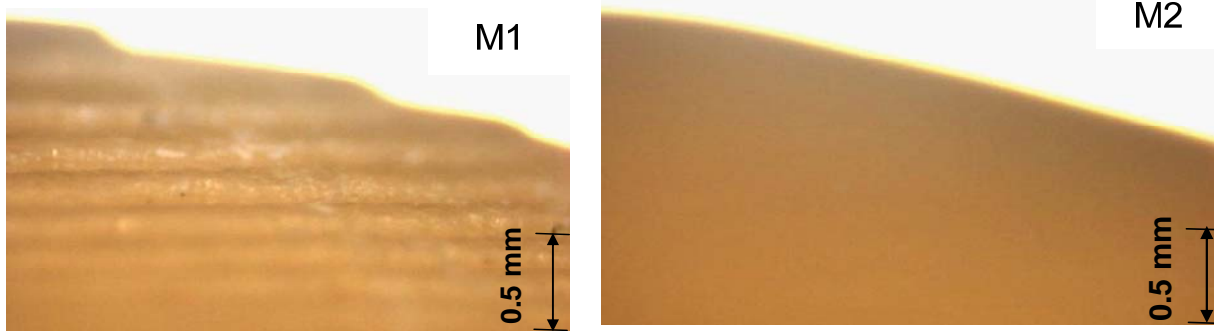
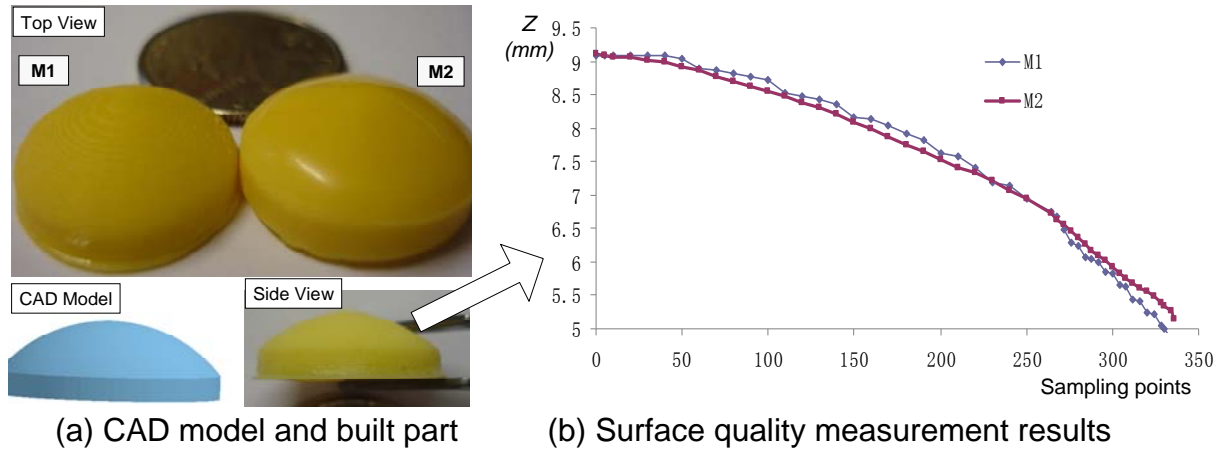


**Figure 17.** A comparison of the built convex up-facing surfaces based on different methods.

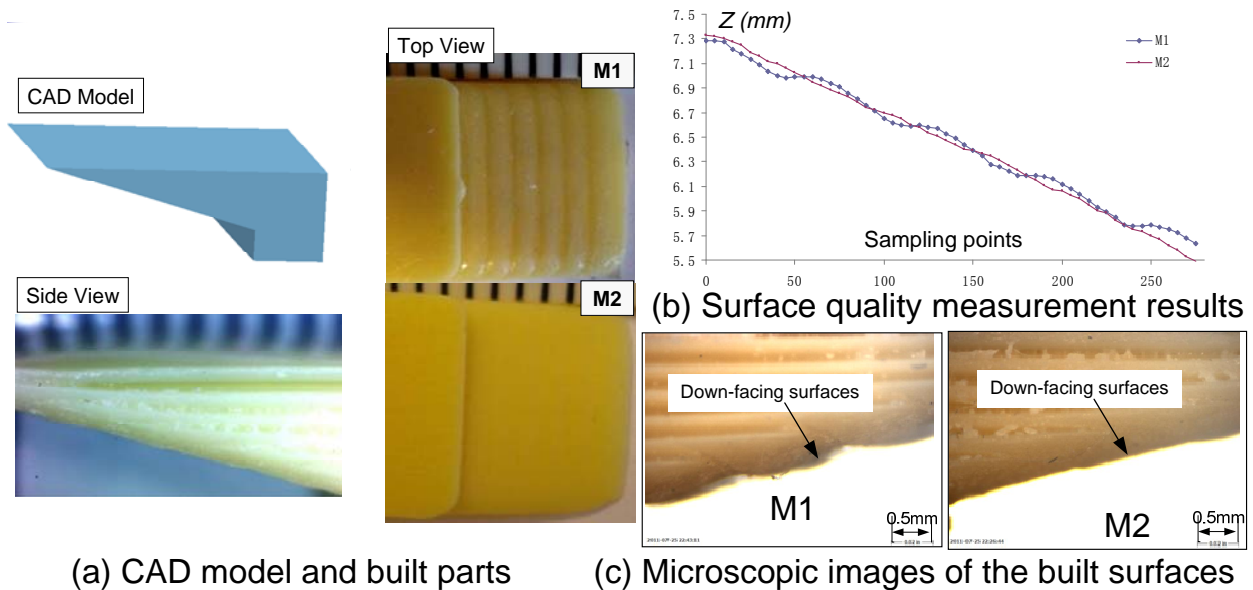


**Figure 18.** A comparison of the built down-facing surfaces based on different methods.

## 8. Conclusions

This paper presented a unique approach to build smooth curved surfaces in the mask-image-projection-based stereolithography process. A meniscus equilibrium method and a grey scale image method have been developed for up-facing and down-facing surfaces respectively. Based on the developed meniscus models in various scenarios, a process planning problem has been formulated for up-facing surfaces. Accordingly an algorithm based on the greedy heuristic was developed for the process planning problem. Based on the calibrated model between curing depths and gray scale values, a process planning algorithm has been developed for down-facing surfaces. Experimental tests based on the developed methods have been performed and compared with the traditional method. The differences in the build results illustrate the effectiveness of our method in improving the surface finish of curved surfaces in the MIP-SL process. Consequently it is possible to build smooth surfaces without sacrificing building time.

The presented method could be further improved to minimize the shape and curvature approximation errors in an up-facing surface. Such improvements can be made by developing better solution strategies for the formulated process planning problem.

## References

1. Elena, D. M., Fuentes, J., Cerro, R. L., and Savage, M. D. (2010), "An analytical solution for a partially wetting puddle and the location of the static contact angle", *Journal of colloid and interface science*, Vol. 348, no. 1, pp. 232-239.
2. Neumann, A.W., Benhabib, B., Szekely, J., Racz, L. M., and Rooks, S. (1991), "Evaluation of two-dimensional and three-dimensional axisymmetric fluid interface shapes with boundary conditions", *Langmuir*, vol. 7, no. 12, pp. 3222-3228.
3. Wayner, P. (1980), "Interfacial profile in the contact line region of a finite contact angle system", *Journal of Colloid and Interface Science*, vol. 77, no. 2, pp. 495-500.
4. Jairazbhoy, V. (1996), "Prediction of equilibrium shapes and pedestal heights of solder joints for leadless chip components", *IEEE Transactions on Components, Packaging, and Manufacturing Technology: Part A*, vol. 19, no. 2, pp. 224-233.
5. Hill, A.I., and Pozrikidis, C. (2011), "On the shape of a hydrostatic meniscus attached to a corrugated plate or wavy cylinder", *Journal of colloid and interface science*, vol. 356, no. 2, pp. 763-774.
6. Rannacher, D., John, T., and Engel, A. (2006), "Influence of surface tension on the conical meniscus of a magnetic fluid in the field of a current-carrying wire", *Journal of Magnetism and Magnetic Materials*, vol. 309, no. 1, pp. 31-35.
7. Adamson, A.W., and Zebib, A. (1980), "Transition region between an infinite plane meniscus and an adsorbed film", *The Journal of Physical Chemistry*, vol. 84, no. 20, pp. 2619-2623.
8. White, L. R. (1977), "On deviations from Young's equation", *Journal of Chemical Society, Faraday Transactions*, Vol. 73, no.1, pp. 390-398.
9. Zisman, W.A. (1964), "Relation of the equilibrium contact angle to liquid and solid constitution" In: R.F. Gould, Editors, *Advances in Chemistry Series 43*, American Chemical Society, Washington, DC, pp. 1-55.
10. Zhou, C., and Chen, Y. (2009), "Three-dimensional digital halftoning for layered manufacturing based on droplets." *Transactions of the North American Manufacturing Research Institution of SME*, Vol. 37, pp. 175-182.
11. Zhou, C. Chen, Y., Waltz, R. A. (2009), "Optimized mask image projection for solid freeform fabrication." *ASME Journal of Manufacturing Science and Engineering*, Vol. 131, No. 6, pp. 061004-1~12, 2009.
12. Jacobs, F. P. (1992). *Rapid Prototyping and Manufacturing: Fundamentals of Stereolithography*, Society of Manufacturing Engineers, Dearborn, MI.
13. Limaye, A. S., and Rosen, R. W. (2007), "Process planning method for mask projection micro-stereolithography." *Rapid Prototyping Journal*, Vol. 13, Iss: 2, pp. 76-84.